Project acronym: MIMO-BRAGG
Spokesperson: Dr. Lorenzo Manti

The objective of the project is to investigate whether sublethal and heritable cytogenetic damage, which is of interest for its impact on long-term healthy tissue morbidity, varies along the penetration depth of charged particles, as described by the Bragg curve. Cellular exposure to ionising radiation is determined not only by the initial amount of damage and unrepaired fraction thereof, but it is also crucially governed by the complexity of such damage, which in turn reflects the peculiar physical pattern with which energy is deposited along and around the particle path., i.e. by its track structure consisting of clusters and spurs of direct and secondary ionizations. Our working hypothesis is that the radiobiological effectiveness of accelerated ion beams, for a given energy, will depend on the particle Z and is therefore only partially describable by the linear energy transfer (LET), the parameter hitherto used to predict the biological effectiveness of radiation types other than photons. Since the track diameter is proportional to the LET but depends on the particle energy and, for a given energy, on the particle Z, the ionisation density will be different between different ions having the same LET. Hence, we intend to study the effects of different ion types and construct "biological" Bragg curves. We requested beam time for three ions that are close enough in Z (oxygen, fluorine and neon) as to irradiate cells along their Bragg curves at positions where the effects of similar LETs could be examined.

We were allocated beam time only for two ion types and carried out two experimental sessions, of 3 BTUs each, one in December 2012, using ^{16}O, and the other in February this year, with ^{20}Ne. The radiobiological endpoints of choice were cellular premature senescence and chromosome aberrations. The former consists of cells entering ectopically (i.e. before physiological exhaustion of their proliferative lifespan) in a permanent growth arrest despite maintaining their metabolic activity, and has been increasingly attracting attention because it can be induced rather efficiently by relatively low doses of particle radiation, hence it represents a potential hazard to hadrontherapy patients, whose normal tissue and/or organs' functionality and homeostasis may be disrupted by accumulation of prematurely senescing cells. Chromosomal aberrations, on the other hand, are a well-known biomarker or cytogenetic damage, which, if inherited by the surviving progeny of irradiated cells, can foster neoplastic transformation. Experimental data on the dependence of such effects on particle type and at different positions of the Bragg curve are lacking. Construction of clonogenic cell death dose-response curves was also planned as they provide reliable information on cellular radiosensitivity,

Accurate dosimetry and Monte-Carlo simulations were planned to provide the physical parameters to which the biological data could be related, and were carried out in collaboration with Dr. Cirrone and his co-workers. The experiments with the 60 MeV/u ^{16}O and ^{20}Ne beams were performed at the 0-degree set-up at LNS. Four different positions were investigated along the pristine Bragg curves (Fig.1). Cells were grown in standard tissue culture flasks and handled prior to and post irradiation at the LNS biology facility. Over 50 samples were irradiated per session. Sample positioning was achieved with resolution less than 50 microns, which greatly reduced the dose uncertainties. For ^{16}O ion irradiation, positions (labeled as P1…P4) corresponded to estimated LET values of 68, 105, 409 and 769 keV/μm, respectively. In the case of irradiation with ^{20}Ne, three of the four positions allowed to irradiate cells with LET values that were very similar to those experienced with ^{16}O ions: these were labeled as P1, P3 and P4, corresponding to estimated LETs of 115, 419 and 764 keV/μm. Position P2 corresponded to an LET value of 189 keV/μm.

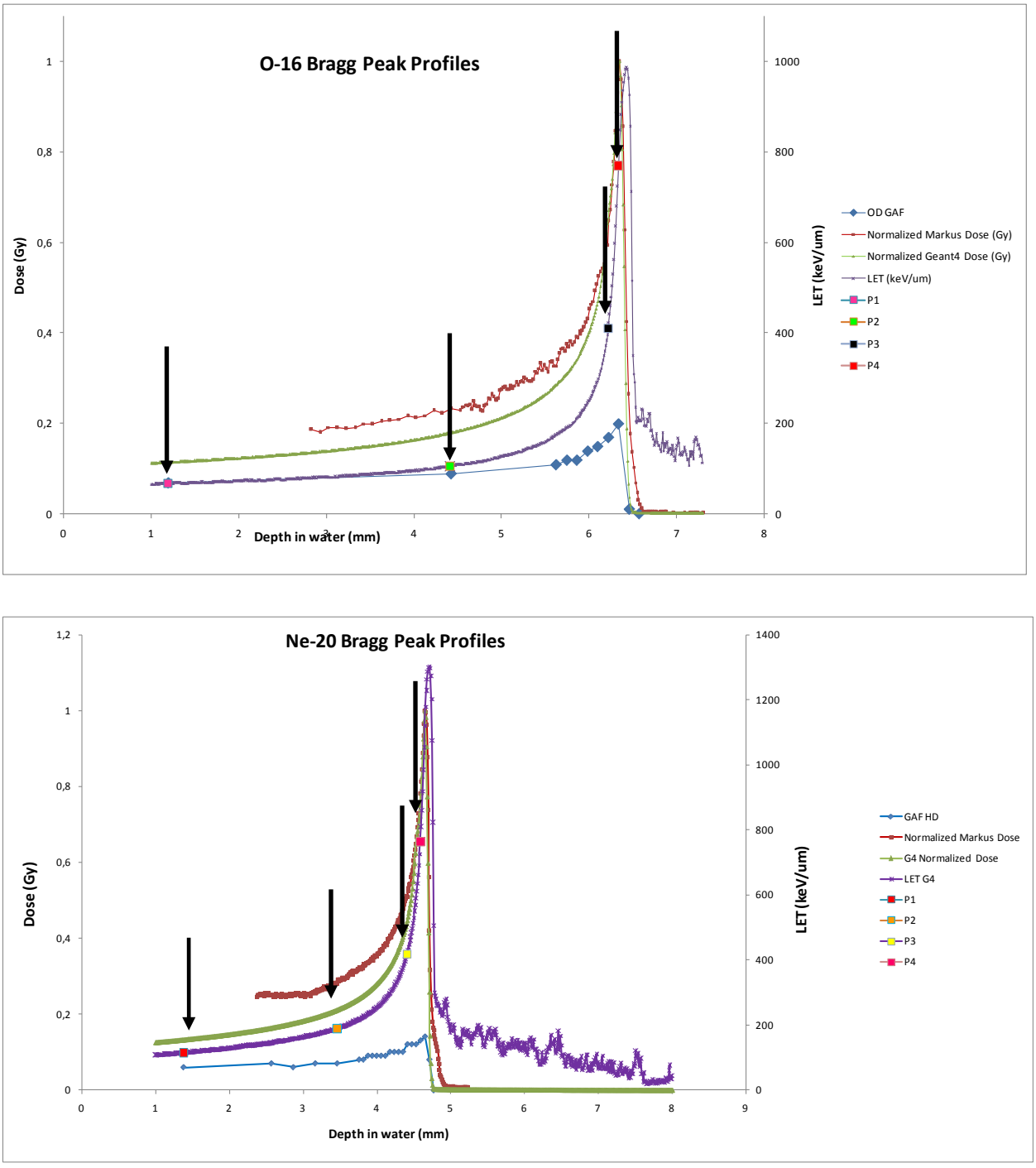

Fig. 1: Dose distributions (Markus chamber) and relative LET values (Geant4 simulations) for the ^{16}O (top) and ^{20}Ne ion beams. Sample positioning (arrows and squares) was verified by optically reading of Gafchromic films and comparing the qualitative dose profile with the quantitative measurements from the Markus chamber.

In this report, complete results are presented from the experiments performed in December 2012 (^{16}O), while preliminary data (senescence and cell survival) are provided from the other session (February 2013, with ^{20}Ne), for which scoring of chromosome aberrations and follow up of cell cultures for measurement of radiation-induced cellular senescence is still under way. Clonogenic

results from the ^{16}O experiment are missing due to post-irradiation culture failure (sub-optimal growth conditions). Part of this work has been used by two final-year MSc. students who discussed their theses (one for the degree in Physics and the other in Applied Biology) earlier this month; a third MSc student is currently working in close association with a PhD student on the implementation of the Monte Carlo-based Geant4 code for the modelization of the ion track structures.

Cellular senescence was studied by means of histochemical detection of β-galactosidase activity, whose expression is peculiar to senescing cells. The assay was performed on cells shortly after irradiation as well as at time intervals for several weeks post-irradiation in order to study both acute and delayed manifestation of this cellular response. Chromosome aberrations were studied by fluorescence *in situ* hybridization (FISH) of chromosome spreads using the method based on calyculin A, which chemically induces chromosome condensation: premature chromosome condensation allows to obtain chromosomes not only from mitosis (as in classical cytogenetic studies), but from any stage of the cell cycle, which avoids the bias of excluding from the analysis those cells that may lag behind the cell cycle due to radiation-induced cell cycle delay, an effect know to occur especially following ion irradiation. Cells for chromosome aberration analysis were harvested 24 hrs after irradiation: at this time repair processes have been completed and the residual mis- or unrepaired damage will be revealed as structural chromosome rearrangements. We used three normal human cell lines, each best suited to study each of the chosen endpoints: fibroblasts (AGO1522) were used for measuring cell survival, endothelial cells (HUVEC) for cellular senescence and epithelial cells (MCF-10A) for chromosome aberrations. In each experimental session, suitable replicates were designed to allow for meaningful statistical analysis.

As for the induction of senescence, low-passage HUVECs were irradiated at the positions as shown in Fig. 1 at two doses (1 and 2.5 Gy). Scoring of senescent cells assayed on 35-mm petri dishes was performed by observation at optical microscope (bright field) on randomly chosen fields. Cells exhibiting a green coloration were identified as positive for β-galactosidase expression (Fig. 2). Between 500 and 1,000 cells per dose and position were scored for all time points examined.

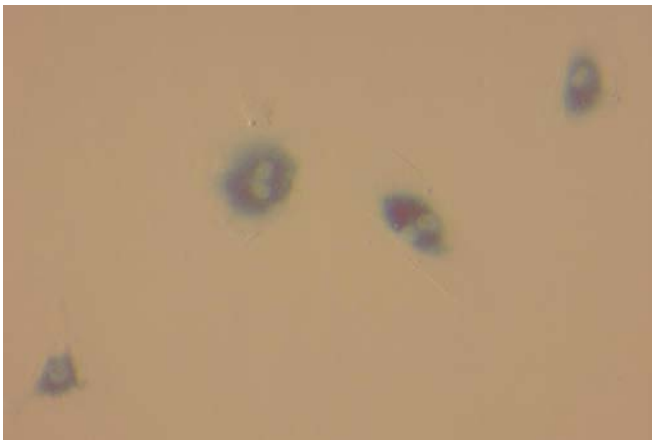

Fig. 2: Example of senescent cells (10X magnification)

In fig. 3 the results obtained for the induction of cellular senescence as a function of time for all doses and positions are shown. The proportion of cells entering physiological senescence gradually increases with time in culture as expected. Radiation causes an increase in the fraction of senescent cells that manifests itself early after exposure and persists until later times. In detail, it is possible to observe an acute response, already manifesting itself at day 1 post-irradiation, with a significantly higher proportion of cells that have entered prematurely senescence among those exposed in P1 (LET of 68 keV/μm). At day 9 the onset of senescence becomes marked for cells exposed closer to the Bragg

peak (i.e. for LET values above 400 keV/μm). At days 26 and 41, cells that were exposed at positions P1 and P2 (lower LET values) exhibited a greater proportion of senescent cells, with the dose of 1 Gy seemingly more efficient than 2.5 Gy. Almost 2 months from irradiation, all cells descending from irradiated cultures showed a higher proportion of senescing cells compared to those from unirradiated cells (control): cells irradiated at positions close to the Bragg peak had similar or slightly higher values of senescence compared to those from P1 and P2.

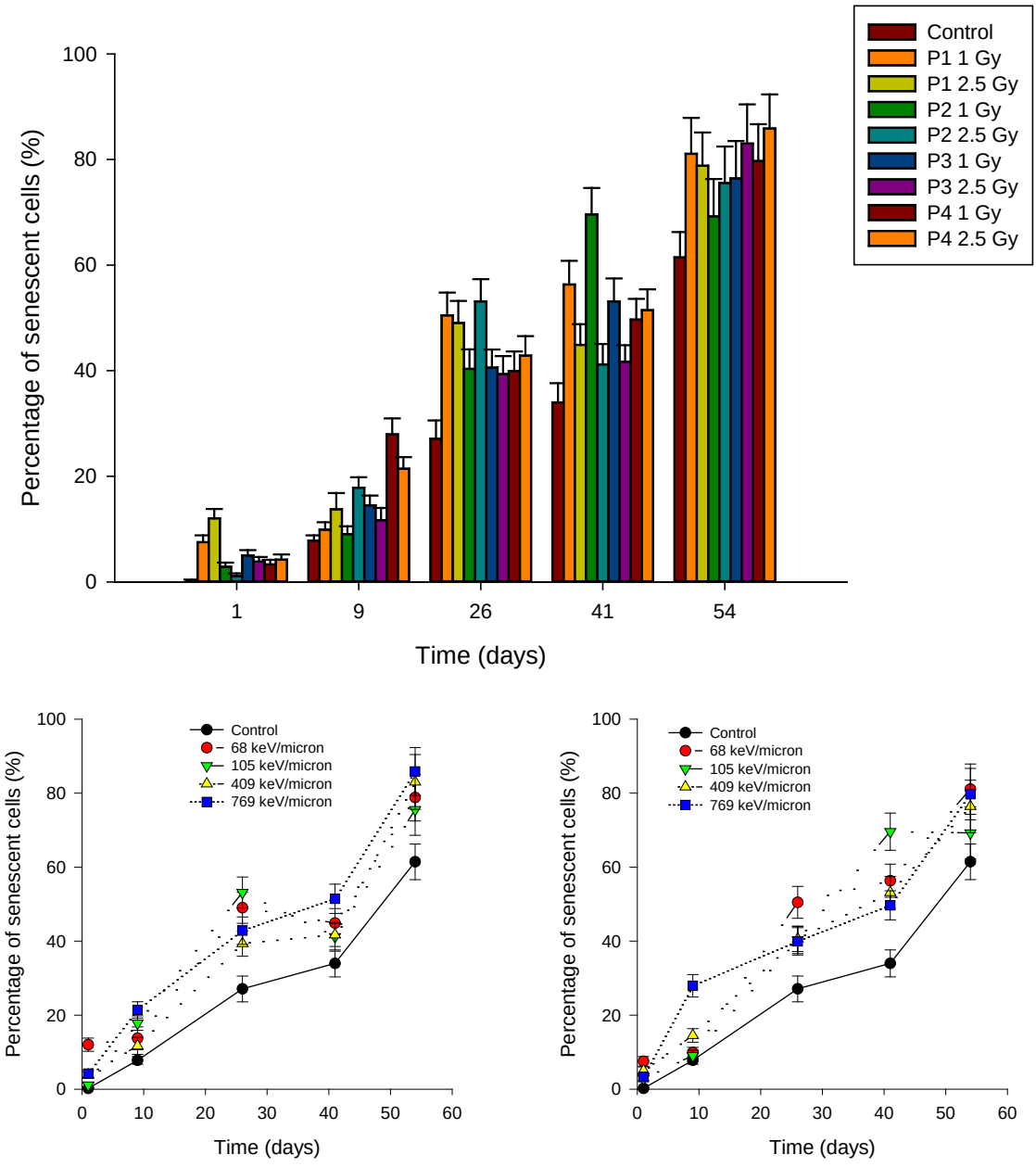

Fig. 3: Induction of senescence by ^{16}O ions: the top graph shows at a glance the time course for all positions and doses; the bottom one shows the time-dependent increase in senescence in cells receiving 2.5 Gy (left) or 1 Gy (right).

The induction of chromosome aberrations by ^{16}O beams was studied in MCF-10A cells exposed in the same positions as illustrated in Fig.1. Cells were given 1 and 2.5 Gy. The FISH technique allows to detects simple and complex exchanges (plus unrejoined fragments) occurring between the stained chromosomes (Fig. 4).

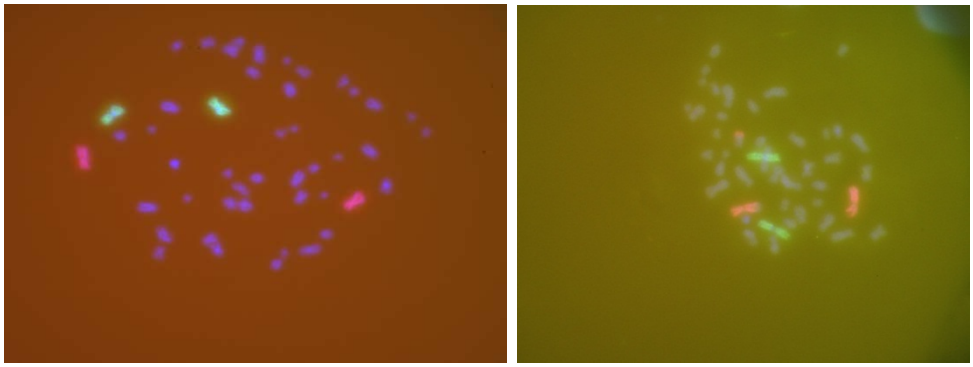

Fig. 4: Example of FISH: chromosomes 1 are painted with a fluorochrome (FITC) green fluorescing when UV illuminated, while the pair of homologue chromosomes 2 fluoresce in red/orange. A normal chromosome spread is shown on the left while an aberrant one exhibiting a translocation is pictured on the right.

In Fig. 5 the fraction of aberrant cells and the frequency of aberrations are reported. The former gives information on the overall efficiency of radiation at causing DNA damage while the latter reflects the damage burden per cell.

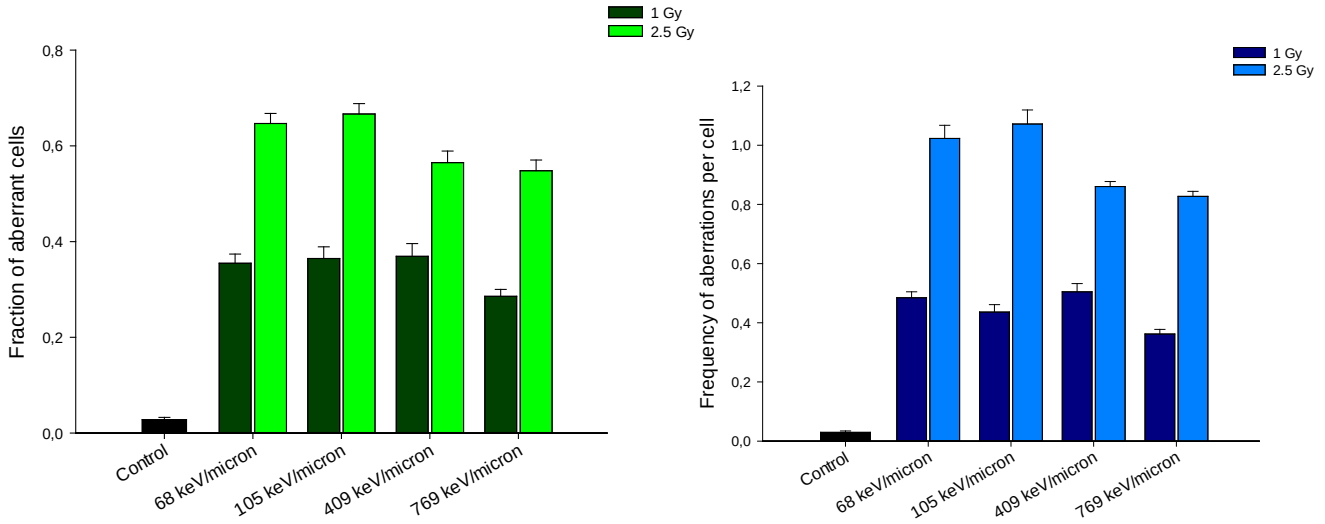

Fig. 5: Proportion of aberrant cells (left) and frequency of aberrations per cell (right) following ^{16}O ion-irradiation

The frequency of complex-type aberrations, which is a know cytogenetic signature of clustered damage, typical of high-LET radiations, is plotted in Fig. 6, alongside the relative contributions to the total aberration counts from the main classes of aberrations scored. The induction of chromosome aberration is clearly dose-dependent, with positions P1 and P2 yielding a higher amount of cytogenetic damage than that measured in cells irradiated close to the Bragg peak (P3 and P4). Even more pronounced is the dependence upon the position along the Bragg curve as far as the yield of complex-type aberrations is concerned (Fig.6).

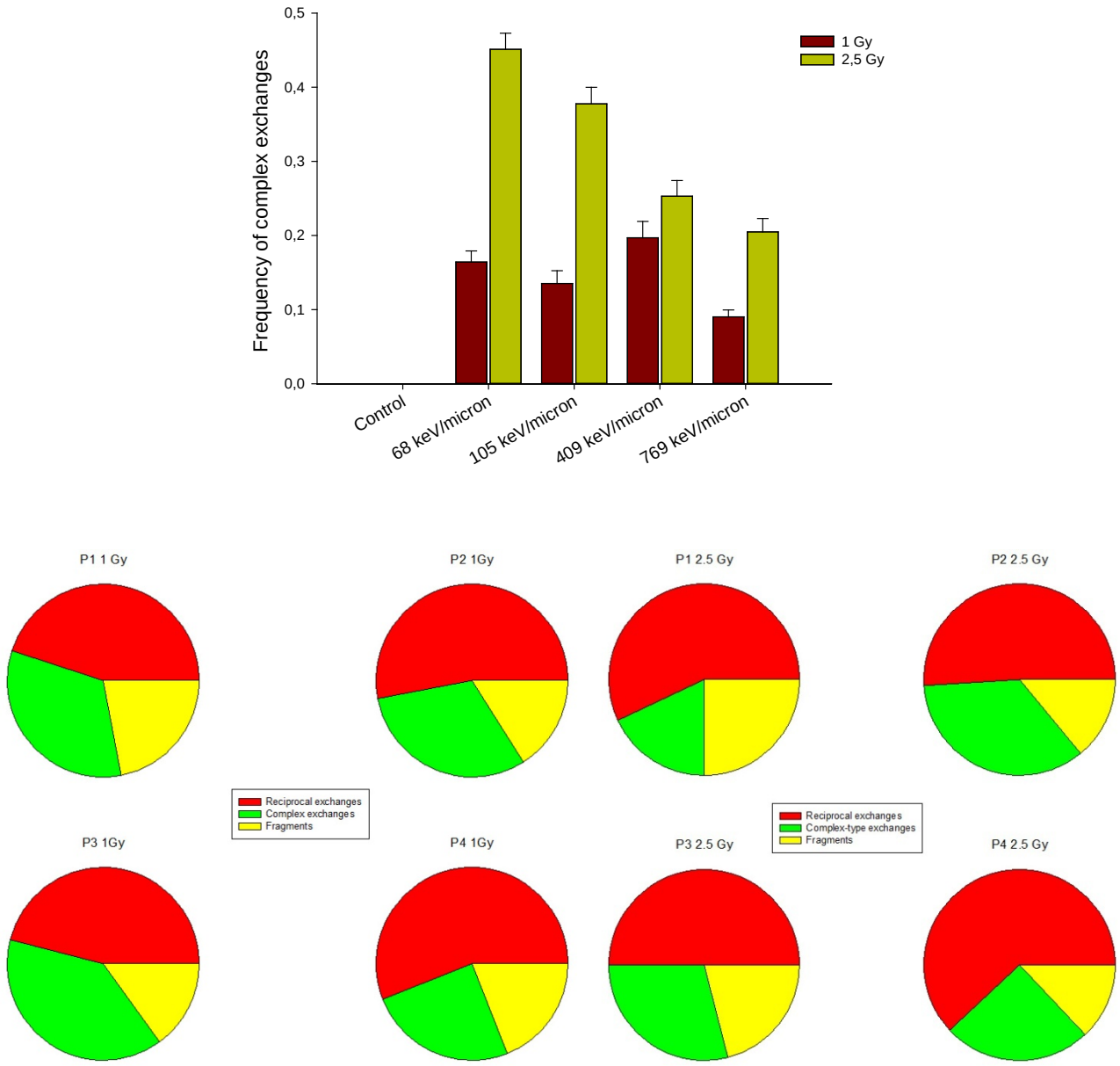

Fig 6: Frequency of complex-type aberrations after ^{16}O ion-irradiation of MCF-10A cells (above). The pie charts show the relative contributions to the overall pool of scored aberrations from three major categories of chromosomal rearrangements, i.e. reciprocal exchanges (red slices), complex-type exchanges (green) and fragments (yellow).

The preponderant type of aberration is represented by simple exchanges; at the highest dose (2.5 Gy) cells exposed in the proximity of the Bragg peak showed a higher incidence of complex-type aberrations compared to those irradiated with 1 Gy in P1 and P2. X-ray induced chromosome aberration data are presented as a comparison in Fig. 7. It can be immediately seen that ions were much more effective at causing chromosome damage than x-rays, particularly as regards the induction of complex-type damage, which was practically negligible in the case of photons. Positions 3 and 4, which resulted the least effective in causing damage following ^{16}O ion-irradiation, were nevertheless three- to four-fold more effective compared to the highest dose (4 Gy) used for low-LET irradiation.

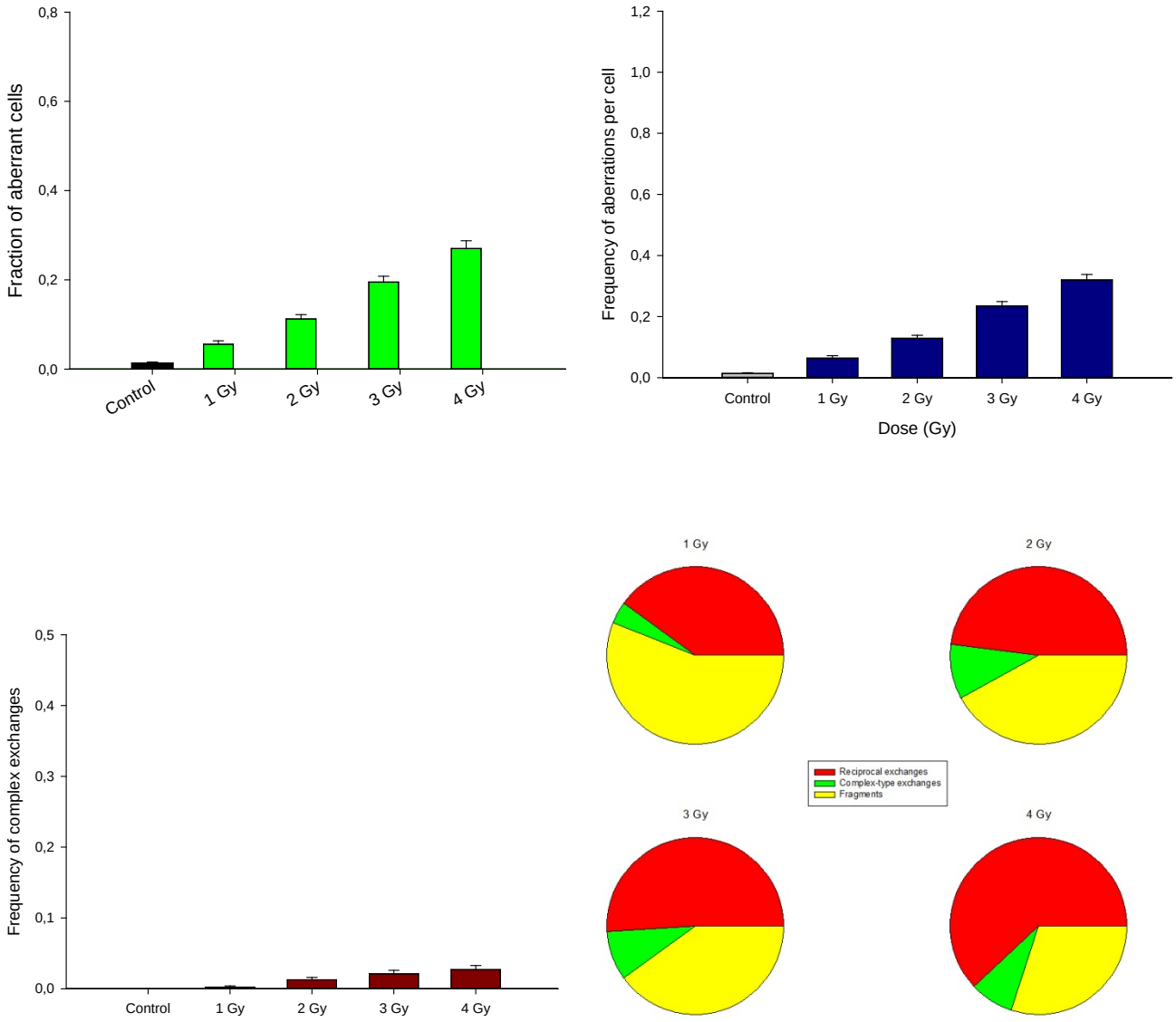

Fig 7: Chromosome aberration induction by x-rays. From top left (clockwise): fraction of aberrant cells; frequency of aberrations per cell; frequency of complex-type aberrations; proportion of reciprocal or complex exchanges and fragments to the aberration catalogue (pie charts).

Clonogenic dose-response curves were derived from ^{20}Ne ion-irradiated fibroblasts as shown in Fig. 8. The more radiosensitive response was yielded by cells exposed in P1, to which an estimated LET of 115 keV/μm was associated. This is in agreement with the expected increase in cell killing efficiency with increasing particle LET (Fig 9). The estimated RBE is about 2.7 at 10% cell survival. Cells exposed at positions P2, P3 and P4, that is at increasing LET values up to a maximum of above 700 keV/μm, did not exhibit any clear difference in their dose-responses. However, the latter showed a significantly more radiosensitive behaviour when compared to x-rays, with an RBE of about 1.3 at the same survival level as above (10%).

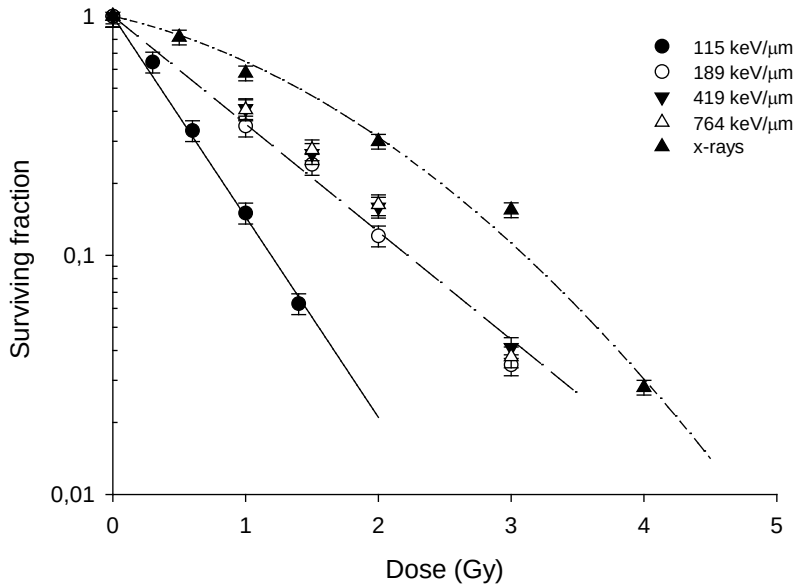

Fig.8: Clonogenic survival curves for AG01522 cells after ^{20}Ne ion irradiation; survival after x-rays (up triangles) is also shown as a comparison.

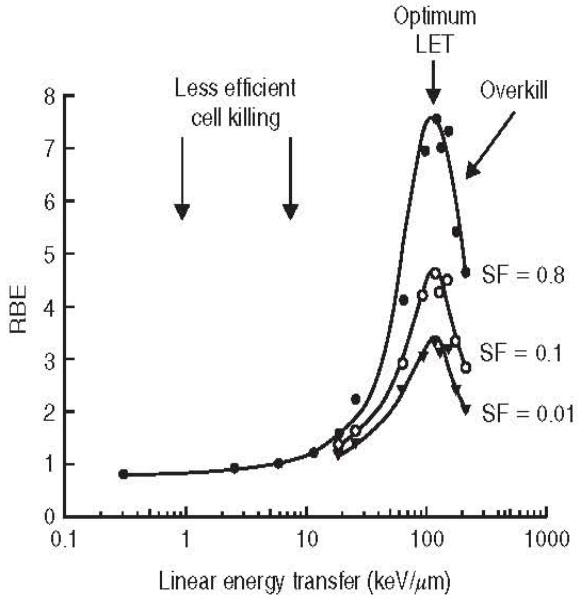

Fig. 9: Classical dependence of RBE upon radiation LET: a similar trend is observed for most radiobiological endpoints although this figure refers to clonogenic survival at different isoeffect levels.

Analysis of cellular senescence following ^{20}Ne ion-irradiation is still under way: data here shown refer to the most recent results obtained at the time of writing (Fig. 10). For practical reasons the sampling times could not be exactly the same as those used in the case of ^{16}O ion-irradiation (Fig.3).

However, it appears that some differences, both qualitative and quantitative, exist when comparing data from the positions corresponding at similar LET values for the two ion types. In particular, it seems that ^{20}Ne is more efficient at inducing cellular senescence, with higher values reached at earlier times, when compared to ^{16}O.

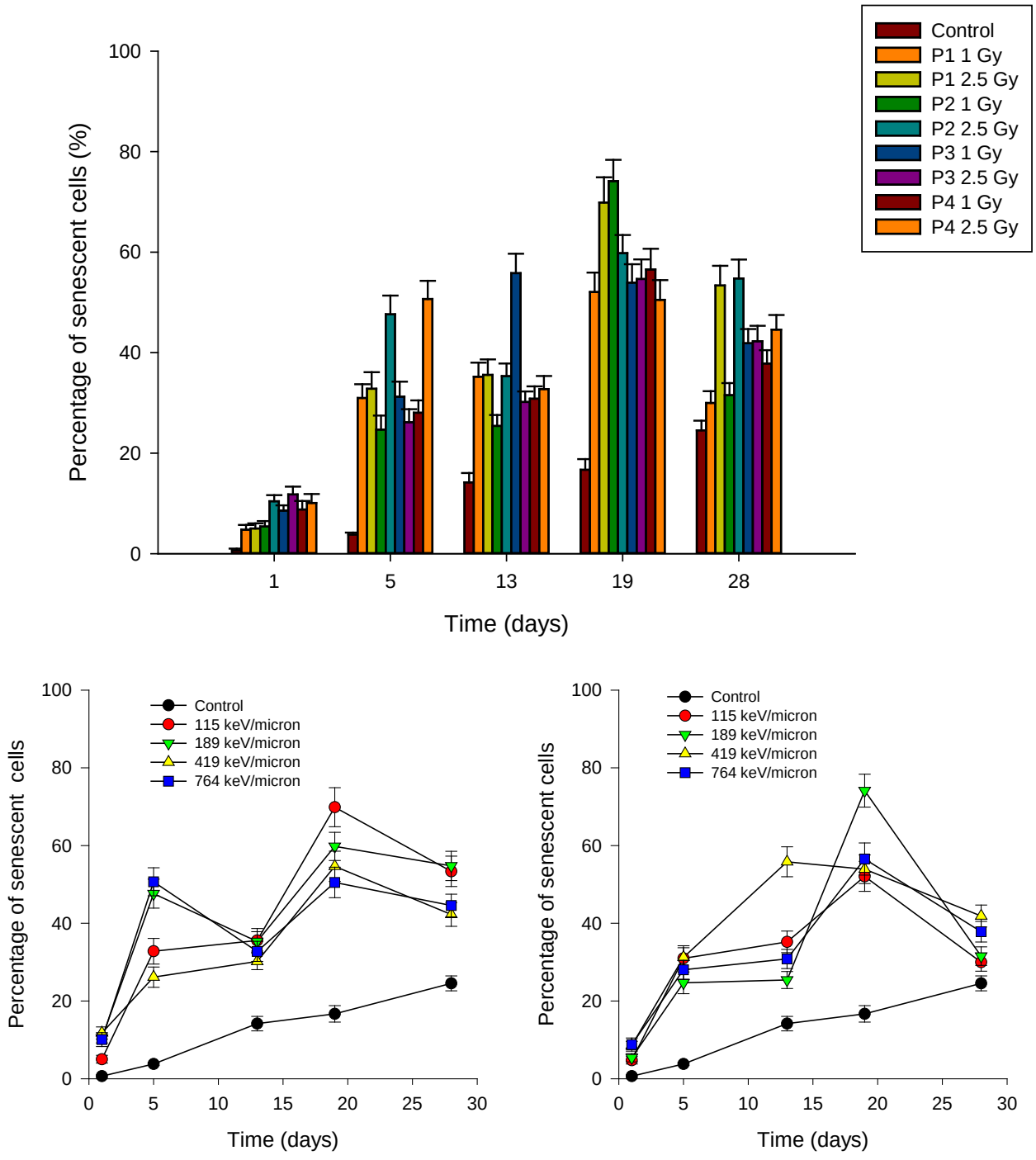

Fig. 10:^{20}Ne ion-induced senescence: the top graph at a glance shows the time course for all positions and doses; the bottom left figure refers to senescence as a function of time post-irradiation after 2.5 Gy while that on the right to 1 Gy (right).

As a comparison, x ray-induced senescence is shown in Fig. 11. It appears that both ^{16}O and ^{20}Ne ions are more effective at causing cellular senescence, even at LET values for which RBE as measured for endpoints that have been more extensively studied (e. g. clonogenic survival, chromosome aberrations, mutations, transformation, etc) would predict similar or even less effective responses (Fig. 9).

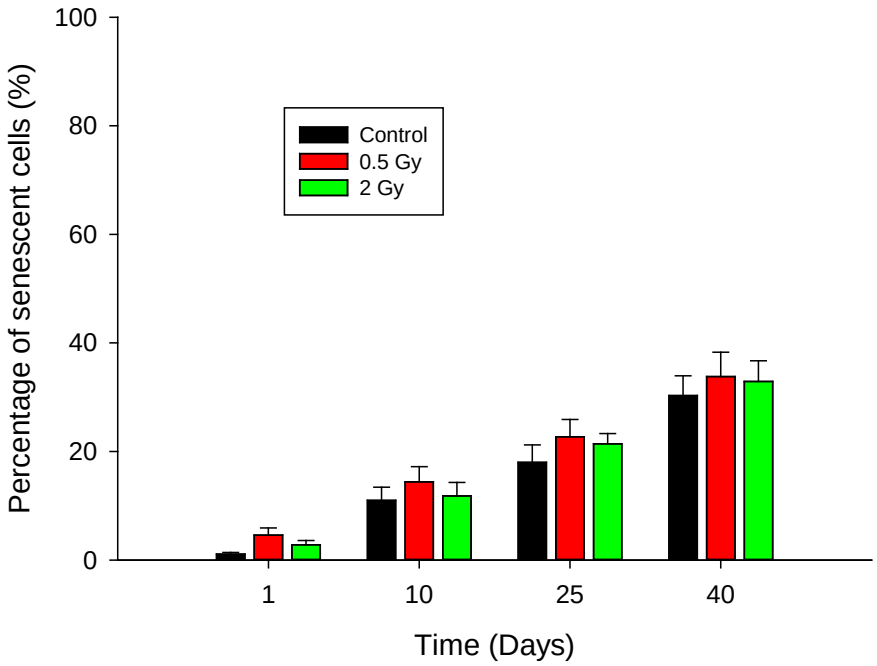

Fig. 11: X ray-induced cellular senescence in HUVEC cell line

In conclusion, senescence data from both ^{16}O and ^{20}Ne ion-irradiations, as well those from chromosome aberrations following ^{16}O ions and clonogenic survival after ^{20}Ne beams, point to significant deviations of particle radiation effectiveness from the behaviour expected solely from radiobiological LET-based models. In particular:

- Cellular senescence is more efficiently caused by ion irradiation compared to photons, and its time course shows qualitative and quantitative dependence upon position along the ion Bragg curve as well as inter-ion differences. Its elevated values immediately after irradiation somewhat question the mere sub-lethal nature of this response, which persists at later times, possibly pointing to a rather different modality of “acute cell death” co-existing with a more orthodox delayed sublethal effect. At very high LET values, i.e. in the close proximity of the Bragg peak, this cellular response is more pronounced and persistent than seen after lower LET values
- Analysis of genetic damage in the form of structural chromosome aberrations confirms that complexity of damage is peculiar to ion irradiation and is much more effectively caused by this type of radiation compared to photons. As also seen for senescence, however, very high LET values, for which radiobiological effectiveness is predicted to decrease significantly, the levels of induced damage are consistently and significantly higher than after low-LET radiation.

- Cell survival analysed after ^{20}Ne ion irradiation confirms that around 100-120 keV/µm cell lethality efficiency reaches its maximum but, rather surprisingly, it also show an RBE greater than unity for cells irradiated close to the Bragg peak.

It is worth to highlight that these are among the first experimental data being produced for endpoints such as cellular senescence and, together with those from chromosome aberration induction, are therefore of value for the construction of "biological Bragg curves" for sublethal cytogenetic damage. This is of interest for normal cells' response, and may contribute to a better understanding of charged particle biological action in contexts such as radioprotection (i.e. indoor radon exposure) and hadrontherapy. These results seem to confirm the inadequacy of LET as the mere physical parameter to predict ion irradiation effectiveness. Before further conclusions may be drawn, it is of course mandatory to corroborate these data with further experiments and to extend such investigation to other ions.

In December 2013 and March 2014 two experimental runs (8 hrs each of beamtime) were carried out at the new hadrontherapy facility in Pavia (CNAO), using a 6-cm SOBP configuration, similar to that used for patients' treatment (Fig. 12). Samples were placed at positions P1, P2, P4 and P5. HUVEC and MCF-10 cell lines were irradiated for assessment of chromosome aberration induction and radiation-induced premature senescence. Data analysis is currently under way.

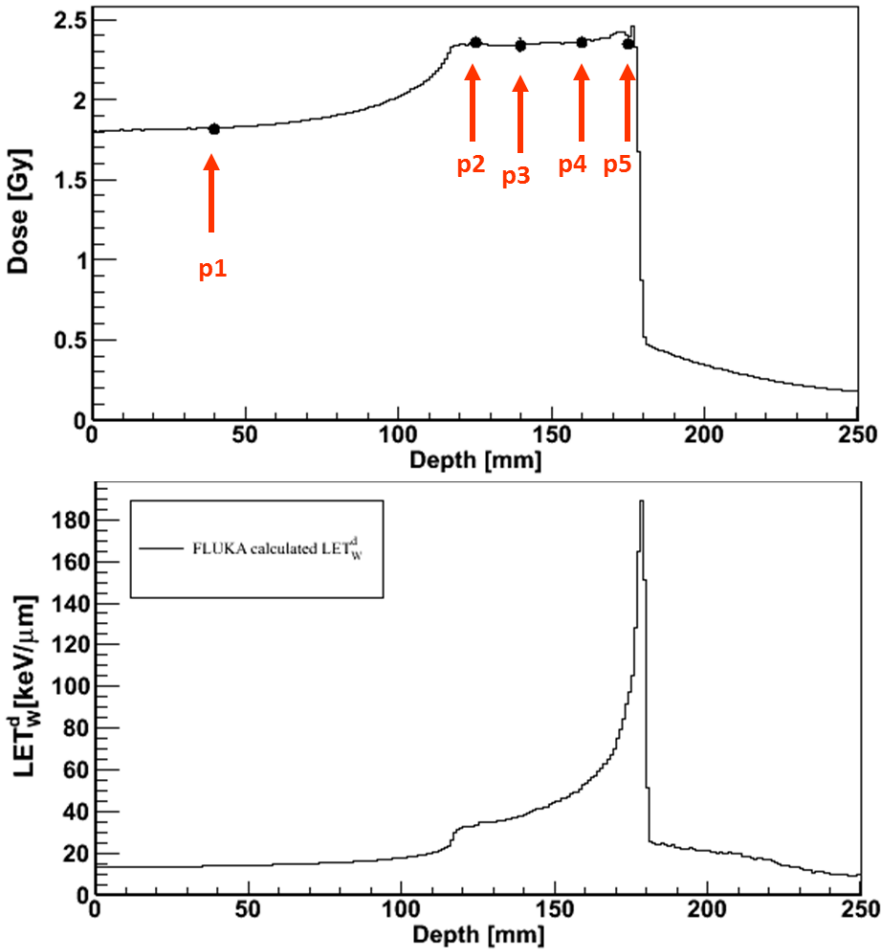

Fig. 12: Dose and LET profiles used for CNAO irradiations. The LET used were 14, 35, 53 and 100 keV/µm (Courtesy of Drs. Ciocca and Mairani, CNAO, Pavia)